IEEE Access
Multidisciplinary ⋮ Rapid Review ⋮ Open Access Journal

Received 20 January 2024, accepted 10 February 2024, date of publication 21 February 2024, date of current version 29 February 2024.

Digital Object Identifier 10.1109/ACCESS.2024.3368762

RESEARCH ARTICLE

Variable Universe Fuzzy PID Control for Active Suspension System With Combination of Chaotic Particle Swarm Optimization and Road Recognition

WANGSHUI YU[1], KAI ZHU[2], AND YATING YU[1]
[1]School of Mechanical Engineering, Jiangsu University of Technology, Changzhou 213000, China
[2]School of Automobile and Traffic Engineering, Jiangsu University of Technology, Changzhou 213000, China

Corresponding author: Kai Zhu (fatkyo@jsut.edu.cn)

This work was supported by the Natural Science Foundation of the Jiangsu Higher Education Institutions of China under Grant 19KJB620001.

ABSTRACT The traditional active suspension system controlled by fuzzy PID fails to consider external road information adaptively, lending to low control precision. To solve this problem, this novel variable universe fuzzy PID control strategy, which combines road recognition and chaotic particle swarm optimization (CPSO), is proposed. Firstly, a dynamic model of four degree of freedom vehicle suspension is established based on the half-vehicle model. Secondly, the Back Propagation (BP) neural network is optimized by Tent Sparrow Search Algorithm (Tent-SSA) to construct a road recognition model. When the road recognition module is constructed, the suspension control system can convert the suspension vibration signal into road information, and dynamically adjust the scaling factors of the variable universe fuzzy controller based on the road information. Thirdly, a modified coefficient is added to adjust the parameters obtained from the road recognition model, and the CPSO algorithm is used to optimize it to enhance control precision. Passive suspension, FPID control, and this novel control are constructed and simulated in MATLAB. The results indicate that this novel control strategy has improved in comprehensive performance by 28.47% compared to fuzzy PID control strategies.

INDEX TERMS Active suspension, CPSO, road recognition, tent sparrow search algorithm.

I. INTRODUCTION

To satisfy the demands of vehicle smoothness and stability, the Active suspension system (ASS) has emerged. The ASS [1], [2] collects road and vehicle status information through sensors and actively generates the control force between tires and vehicle by actuator based on control strategy. Therefore, the main object of this paper is constructing an exemplary active suspension control strategy to improve the passenger comfort, and enhance road adhesion.

Many academics and researchers have put forward various control strategies for active suspension in vehicles, such as adaptive PID control [3], [4], fuzzy control [5], neural network [6], [7], Intelligence Algorithms [8], etc. However, vehicles face complex and random road excitations in actual driving, which necessitate the suspension control system to accurately and rapidly respond to the road excitation in order to enhance suspension control performance. To address the time delay and uncertainties in road excitations, a novel adaptive fuzzy control method [9] offered for managing suspension system through a delay compensation strategy. This approach effectively minimized the impact of road information delays on the ASS. A fixed-frequency controller [10] emerged using a PSO technique, Dynamic vibration absorber parameters, and linear quadratic regulator (LQR) controller weighting factors to suppress the vibrations of generated by vehicle traveling on various road frequencies. The adaptive fuzzy PID control strategy [11] achieved

The associate editor coordinating the review of this manuscript and approving it for publication was Wei Quan.

smoother suspension control by employing fuzzy processing in response the uncertainty of road surfaces. Machine learning [12] was employed for the transformation of in-vehicle sensor information, enabling accurate conversion of vehicular data into road surface roughness. Genetic algorithms [13] were employed to optimize the active suspension control parameters, aiming to minimize the extreme accelerations experienced by the passenger seat due to severe road conditions.

To achieve the better suspension control, it is required to research comprehensive controllers. To address the issue of unpredictable optimal damping force generated by road excitations in the suspension system, a PID controller with the advanced firefly algorithm tuning was investigated [14]. The neural networks [15] by adding feedback connections between output and input layers can effectively applied as a part of vehicle system model to accurately predict road excitations and tire dynamics behavior. The Recurrent Neural Network and Long short-term memory neural network [16] were employed the to ensure the stability of vehicles suspension under all external or internal conditions.

The above literature elaborated on the impact of road excitation on suspension and proposed their respective solutions. This paper proposes to combine intelligent algorithms with fuzzy control to address this issue, which constructs a variable universe fuzzy PID (VUFP) control strategy with road recognition (RR) and chaotic particle swarm optimization (CPSO) to effectively handle road variations and PID parameter adjustments, improving control performance. The higher control performance will ensure energy utilization efficiency.

Following are the primary contributions made by this paper:

1. The RR module is employed to address the drawback of a fixed universe in fuzzy control and overcome complex road excitation. Firstly, multiple vehicle speeds and sprung masses are used to run on various road surfaces, generating an enormous quantity of data. The Tent-SSA-BP neural network's structure and parameters are trained using this data as input training set. This neural network is capable of converting suspension performance signals into road information. Subsequently, the road information is passed to the constructed VUFP control system. This control system outputs the required PID control parameters, effectively overcoming the limitations of a fixed universe.

2. A CPSO optimization system is designed, which introduces PID correction coefficients to adjust the PID control coefficients and utilizes the CPSO strategy for optimization. Taking into consideration the various performance requirements of the suspension, this strategy can further enhance control precision, and respond more rapidly to differences in control performance and road conditions. This ensures the comfort and operability of vehicle travel under different road conditions.

The rest of the article is organized as follows: Section II presents the construction of the dynamic model and the suspension actuator. Section III focuses on the overall framework and goals of the control strategy design. It covers topics such as the design process of variable-domain control, the principle of Tent-SSA, the construction of road recognition system and CPSO. Section IV conducts simulation experiments and compares the vibration reduction effects of several different control strategies, clearly demonstrating the vibration reduction effect of the control strategy proposed. Section V illustrates the conclusions drawn from the experimental results obtained in this study.

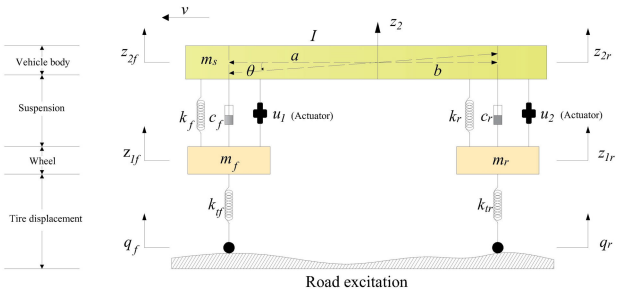

FIGURE 1. Four DOF 1/2 vehicle model.

II. ACTIVE SUSPENSION SYSTEM

A. DYNAMIC MODEL OF ACTIVE SUSPENSION

Considering that the 2 degree of freedom (DOF) 1/4 body only reflects the vertical motion of the vehicle and cannot display the pitch motion. Meanwhile, the computational complexity is too large when using the 7 DOF body as the model. Therefore, this article establishes a 4 DOF 1/2 vehicle active suspension model as the research object. Fig.1 depicts the suspension model.

In Fig.1, z_2, θ, m_s, I respectively indicate the vertical displacement, pitch angular, mass, and the inertial moment at the vehicle body. a, b represent the distances from the front and rear suspension axes to the center of the vehicle body. m_f, k_f, c_f symbolize the sprung mass, stiffness coefficient, and damping coefficient. z_{1f}, z_{2f} depict the vertical displacement of unsprung mass and sprung mass of the front suspension, respectively. m_r, k_r, c_r stand for the sprung mass, stiffness coefficient, and damping coefficient. z_{1r}, z_{2r} illustrate the vertical displacement of unsprung mass and sprung mass of the rear suspension, respectively. q_f, q_r signify the road excitation. The active suspension control force (u_1, u_2) generated by the actuator.

In this model, the front and rear sprung masses' vertical displacements and the spring masses' vertical displacement at the center of gravity are connected in the following formula, assuming that the θ is extremely tiny (near zero):

$$z_{2f} = z_2 - a\tan\theta \approx z_2 - a\theta \tag{1}$$

$$z_{2r} = z_2 + b\tan\theta \approx z_2 + b\theta \tag{2}$$

When the tires maintain contact with the road, the vehicle suspension system is expressed as follows:

$$\begin{cases} F = M_t\ddot{Z}_{fr} - K_sZ_t + K_t(Z_{fr} - q) \\ AF = M_u\ddot{Q} - AK_sZ_t \end{cases} \tag{3}$$

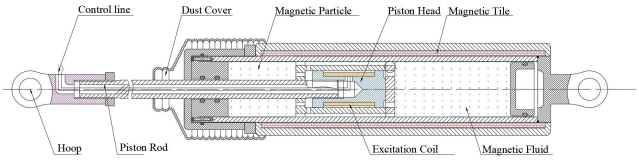

FIGURE 2. The Structure of MRD.

Define $\ddot{Z}_{fr} = [\ddot{z}_{1f}\ \ddot{z}_{1r}]^T, \ddot{Q} = [\ddot{z}_2\ \ddot{\theta}]^T, F = \begin{bmatrix} u_1\ u_2 \end{bmatrix}^T$ the corresponding matrices:

$$M_t = \begin{bmatrix} m_f & 0 \\ 0 & m_r \end{bmatrix}, M_u = \begin{bmatrix} m_s & 0 \\ 0 & I \end{bmatrix}, K_s = \begin{bmatrix} k_f & 0 \\ 0 & k_r \end{bmatrix},$$
$$K_t = \begin{bmatrix} k_{tf} & 0 \\ 0 & k_{tr} \end{bmatrix}, A = \begin{bmatrix} -1 & -1 \\ a & -b \end{bmatrix}$$

To comprehensively compare the control performance of the vehicle, taking into account ride comfort, handling, and suspension safety, the following objective function is defined:

$$J = \min(RMS[\ddot{z}_2] + RMS[\ddot{\theta}] + RMS[\Delta x]) \qquad (4)$$

where RMS is Root Mean Square, $\ddot{z}_2$ represents the vehicle body's vertical acceleration (VBVA), which is associated with the ride quality. A lower value indicates better ride comfort. The $\ddot{\theta}$ stands for the vehicle body's pitch angular acceleration (PAA), which affects the handing. A smaller angle depicts smoother driving and better handing. The $\Delta x = z_{2f} - z_{1f}$ symbolizes the front suspension displacement (FSD), and its value shows whether the suspension is operating within the normal range. If the value exceeds the reasonable range, it displays that the suspension may be damaged and needs replacement. The complete assessment aims to improve ride comfort, enhance vehicle maneuver's ability, and guarantee the suspension system's correct operation.

B. THE SUSPENSION ACTUATOR

This paper adopts magnetorheological damper (MRD) as the suspension actuators for smooth control [17], [18]. The structure of the MRD, as illustrated in Fig.2, includes the Hoop, Control line, Piston Rod, Magnetic Particle, Excitation Coil and Magnetic Fluid, among other.

The operating principle of the MRD is as follows:

(a) In the absence of MRD operation, the Magnetic Particle are randomly dispersed within the Magnetic Fluid, allowing the damping orifice to remain unblocked. At this moment, the damping force of the MRD is relatively low. The internal changes of the MRD are depicted in Fig.3(a).

(b) When the MRD is energized, Magnetic Particles aggregate near the excitation coil due to the influence of the Magnetic field. This aggregation leads to the blocking of the damping orifice, preventing the fluid from moving rapidly and causing a significant increase in the damping force. Furthermore, as the electrical current increases, it generates a stronger magnetic field, resulting in greater attraction of suspended particles and a higher damping force. The internal changes of the MRD are portrayed in Fig. 3(b).

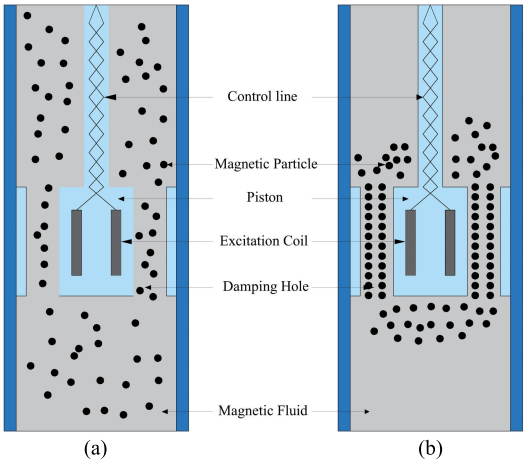

FIGURE 3. The MRD state; (a) Not energized state; (b) Energized state.

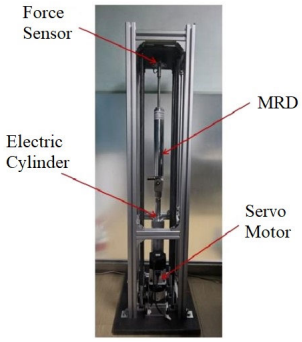

FIGURE 4. The testing apparatus.

To better illustrate the performance of the MRD, this study employs the vertical sinusoidal motion of an electric cylinder as the displacement excitation, with a sine wave frequency of 2Hz and an amplitude of 15mm. The coil diameter of the MRD is 0.5mm, and the six different currents are applied: 0A,0.2A,0.4A,0.8A,1A, and 1.2A. The testing apparatus is displayed in Fig.4. The relationship between damping force and piston displacement are depicted in Fig. 5(a).

The working principle of the MRD is to altering the excitation current, causing a change in the magnetic field, and changing the properties of the magneto rheological fluid to obtain the required damping force. Based on Faraday's electromagnetic induction law, the changing magnetic field in the coil will generate induced electromotive force inside the copper core, leading to the generation of eddy currents. The eddy currents are always opposite to the magnetic field induced by the excitation current. So, it will hinder the variation of the magnetic field excited by the excitation current, leading to a lag in the control response time. This lag affects the control performance of the active suspension system. Table 1 shows the response time and damping force results under different currents. Fig.5(b) illustrates the relationship between response time and current variation.

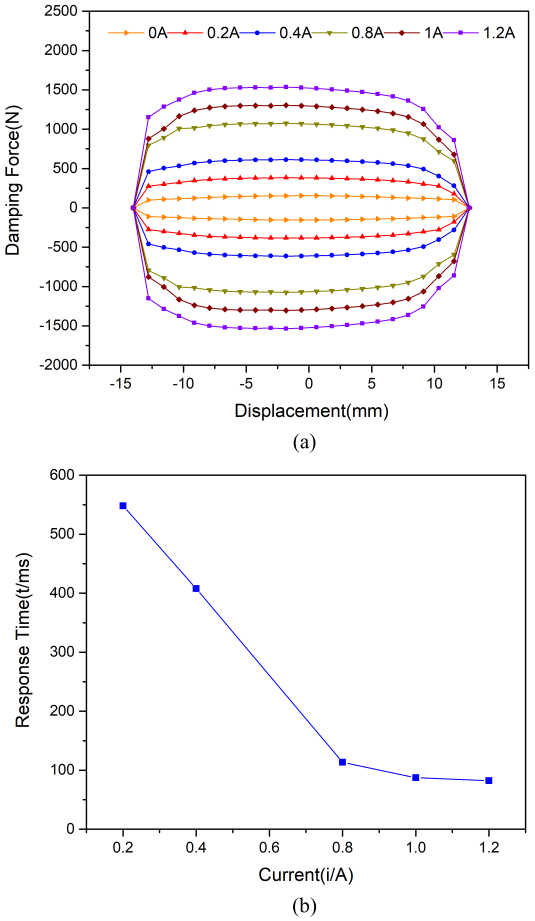

FIGURE 5. (a) The relationship between damping force and piston displacement; (b) the relationship between response time and current variation.

TABLE 1. The response time and damping force result.

Current (i/A)	Response Time (t/ms)	Damping Force (N)
0	\	136.798
0.2	548.17	341.310
0.4	407.86	550.012
0.8	113.46	975.416
1.0	87.34	1172.976
1.2	82.14	1394.77

When the MRD unpowered, the damping force of the MRD is approximately 136N. As the current continues to increase, the damping force also continues to increase. Evidently, as the current continuously increases, the excitation coil's magnetic field intensifies, leading to a deeper aggregation of suspended particles and a progressive increase in the damping force of the MRD. Furthermore, the damping control of the MRD appears relatively stable, with minimal damping fluctuations.

Meanwhile, within the current range of 0-0.8A, as the current value increases, the response time decreases significantly. However, within the range of 0.8-1.2A, the reduction in response time is not significant. This indicates that during active suspension control, there is still a certain lag in the control due to the influence of the characteristics of magneto rheological dampers, which reduces control efficiency.

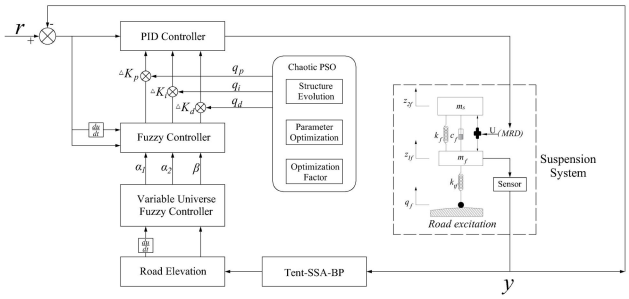

FIGURE 6. The framework for the control strategy.

III. CONTROL STRATEGY

Fig.6 respectively display the framework of the control strategy. Firstly, sensors receive the signals from the suspension system. Then, these suspension signals are input into the Road Recognition Module based on the Tent-SSA-BP neural network, from which the road grade (G) and road membership degree (ΔG). Subsequently, both signals are forwarded to the variable universe controller. The controller outputs the scaling factor to adjust the domain of the fuzzy controller. In this process, both the suspension vibration signal and error signal are fed into the fuzzy controller, which outputs the three control parameters (ΔK_p, ΔK_i, ΔK_d) for the PID. This not only allows the control system to adaptively adjust based on road information but also enhances the precision of the output parameters.

The primary purpose of the CPSO Optimization module is to tune the PID output parameters for more accurate control. First of all, the sensors receive suspension performance signals to generate the initial PID parameters (K_p, K_i, K_d). Meanwhile, the PID correction coefficients (q_p, q_i, q_d) are combined with the RR module's output parameters.

$$\begin{cases} K_{P0} = K_P + \Delta K_P \times q_p \\ K_{i0} = K_i + \Delta K_i \times q_i \\ K_{d0} = K_d + \Delta K_d \times q_d \end{cases} \tag{5}$$

Then, CPSO is employed to continuously optimize the PID correction coefficients, enabling real-time adjustment of the PID control parameters and ensuring precise control.

A. DESIGN OF VARIABLE UNIVERSE FUZZY

The variable universe is designed to adjust the Fuzzy controller's domain and overcome the limitations of the fixed domain. This enables the controller to respond to varying road conditions, providing a more precise and effective control range. Its essence lies in changing the primary universe of input and output in a specific rule according to the control

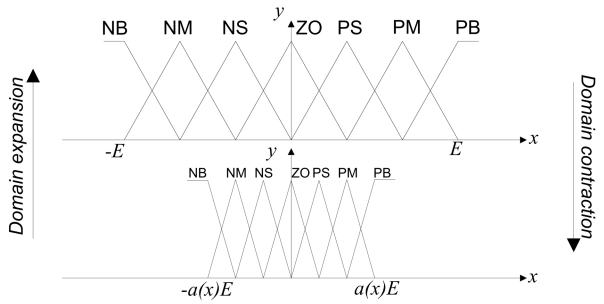

FIGURE 7. The variation of contraction-expansion universe.

requirements. Therefore, the influence of expert expertise on the design of the variable domain fuzzy controller is greatly reduced, resulting in increased accuracy.

This specific design concept is as follows:

1. When $id = [-E_i, E_i]$, $od = [-U_i, U_i](i = 1, 2, \ldots, n)$ represent the input domain (id) and output domain (od), respectively. IR, OR indicate the input fuzzy rule and fuzzy rule output. Meanwhile, i denotes the index of the i-th input value, j shows the index of the j-th interval in the fuzzy rule partitioning.

2. The input and output domains can change along with contraction-expansion factors, which are expressed by the following formulas:

$$\begin{cases} id_i = [-\alpha_i E_i, \alpha_i E_i] \\ od = [-\beta U_i, \beta U_i] \end{cases} \tag{6}$$

where α_i, β respectively refer to the contraction-expansion factors the input universe and output universe.

Fig.7 demonstrates how the contraction-expansion factors modify the universes. The process involves the fuzzy subset related to the scaling factor of input ($[-E, E]$) generating new domains ($[-\alpha E, \alpha E]$).

The mathematical expressions for these contraction-expansion factors are typically represented as follows:

$$\alpha = 1 - \lambda e^{-ke(t)^2} \tag{7}$$

$$\beta = k_i \sum_{i=1}^{n} P_i \int_0^t e_i(t) d_t + \beta(0) \tag{8}$$

where $e(t)$ is the input variable, λ, k, k_i are the contraction-expansion factor coefficient, index coefficient, and the constant of integration. P_i is the weight constant vector, $\beta(0)$ is the initial value 1 [19].

3. In this study, the selection of parameters for the controller's input and output, along with the construction of corresponding fuzzy control rules, is as follows: Road grade (G) and road membership degree (ΔG) are chosen as the control input variables. The α, β are selected as the output variable. There are seven main categories for normal road grades: A, B, C, D, E, F, and E. Generally, vehicle travel on roads classified as A to D. Therefore, in this study, the fuzzy domain of the input variable is set to {-0.07,0.07} and divided into seven intervals, including {NB (Negative Big), NS (Negative Small), ZO (Zero), PS (Positive Small), PM (Positive Medium), PB (Positive Big)}, represented by Gaussian membership functions [20].

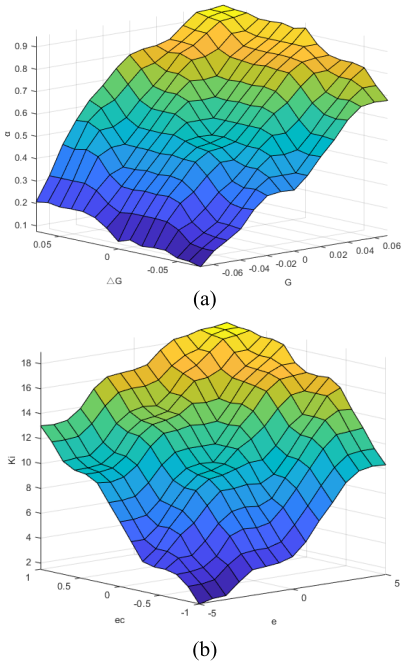

FIGURE 8. (a) The visualization of contraction-expansion factor; (b) The visualization of control rules of the fuzzy controller.

TABLE 2. The fuzzy rules of contraction-expansion factor.

α_1	ΔG							
	NB	NM	NS	ZO	PS	PM	PB	NB
	NB	PB	PB	PM	PM	PS	ZO	ZO
	NM	PB	PB	PM	PS	PS	ZO	NS
	NS	PM	PM	PM	PS	ZO	NS	NS
G	ZO	PM	PM	PS	ZO	NS	NM	NM
	PS	PS	PS	ZO	NS	NS	NM	NM
	PM	PS	ZO	NS	NM	NM	NM	NB
	PB	ZO	ZO	NM	NM	NM	NB	NB

AS illustrated in Table 2, when G, ΔG are NB, it displays that the vehicle is running smoothly, and the required control force isn't excessive. Consequently, the contraction-expansion factor α is also set to NB. However, when G, ΔG are PB, it exhibits that the vehicle is travelling on uneven ground, necessitating an increased control force to offset the force caused by vibration. As a result, the contraction-expansion factor α is likewise set to PB. Table 2 lists the control rules for contraction-expansion factors. Fig. 8(a) presents the visualization of contraction-expansion factor.

TABLE 3. The fuzzy rules of variable domain.

ΔK_i	ec							
	NB	NM	NS	ZO	PS	PM	PB	NB
e	NB	PB	PB	PM	PM	PS	ZO	ZO
	NM	PB	PB	PM	PS	PS	ZO	NS
	NS	PM	PM	PM	PS	ZO	NS	NS
	ZO	PM	PM	PS	ZO	NS	NM	NM
	PS	PS	PS	ZO	NS	NS	NM	NM
	PM	PS	ZO	NS	NM	NM	NM	NB
	PB	ZO	ZO	NM	NM	NM	NB	NB

TABLE 4. The road surface grade parameters.

Road Grade	$G_q(n_0)/10^{-6}m^3$	Road Grade	$G_q(n_0)/10^{-6}m^3$
A	16	E	4096
B	64	F	16384
C	256	G	65536
D	1024	H	262144

The above statement explains how the variable universe adjusts the fuzzy controller domain based on the road information. The fuzzy controller outputs PID control parameters (ΔK_p, ΔK_i, ΔK_d) based on the same principle when it receiving suspension vibration signal and error signals. Table 3 presents the control rules of the fuzzy controller. Fig.8(b) shows the visualization of control rules of the fuzzy controller.

B. DESIGN OF ROAD RECOGNITION

Random road excitation is a primary factor that affects the vibration of vehicle suspension. In this paper, a harmonic superposition method is used to construct a road roughness model. The simulated time-domain model of the road disturbance is specified as follows [21]:

$$\dot{q}(t) = -2\pi f_0 v q(t) + 2\pi n_0 \sqrt{G_{q(n_0)}} v w(t) \tag{9}$$

where $w(t)$ is a Gaussian white noise, v is vehicle speed value, n, n_0 respectively are the spatial frequency and reference spatial frequency, $G_q(n_0)$ is the road roughness factor, $f_0 = 0.01m^{-1}$, $q(t)$ is the road excitation.

Based on international standards, the road roughness is generally divided into 8 levels [22], as shown in the Table 4.

This article translates suspension dynamic parameters ($\ddot{z}_2, \ddot{\theta}, \Delta x$) into road surface information ($q(t)$). The BP neural network [7], [23], [24] boasts versatile advantages, dynamically adjusting weights and thresholds to accommodate intricate patterns and relationships within input data. Meanwhile, BP neural network excels in modeling complex relationships, and its parallel processing architecture

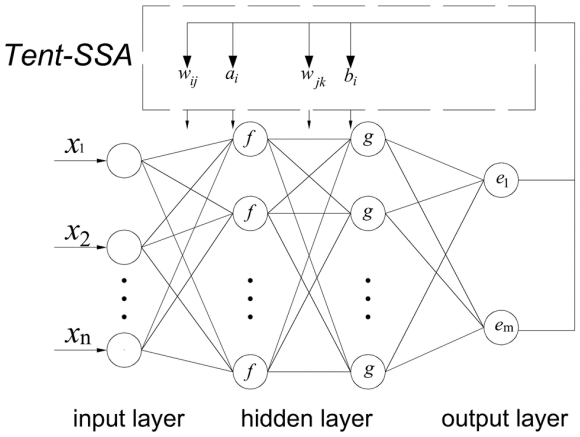

FIGURE 9. The structure of Tent-SSA-BP.

enhances training and prediction efficiency. Based on the aforementioned advantages, this paper adopts the BP neural network as the foundation for the road recognition model.

To optimize the BP neural network, this paper introduces Tent-SSA to optimize the weights and thresholds parameters of the BP neural network. Tent-SSA-BP neural network, whose architecture is depicted in Fig.9. An input layer, two hidden layers, and an output layer make up its four layers. It has the characteristics of error back-propagation and weight coefficient modification are performed continuously. The weights are continuously modified by the Tent-SSA approach to minimize the RMS error between the network's actual output values and desired output values in order to reduce overall network error.

The SSA (Sparrow Search Algorithm) [25]was proposed in 2020. Compared to other algorithms like Bat, Grey Wolf, or Ant, SSA exhibits superior global search performance, especially in exploring different search spaces. It efficiently addresses the issue of local optima that arises during nonlinear problem-solving processes. However, SSA tends to exhibit sparrow flocking behavior at the initial stage. To overcome this, the chaotic algorithm "Tent" is introduced to resolve the initial clustering phenomenon in the SSA algorithm.

The main rules of SSA are as follows:

The sparrow population is mainly divided into three categories: Discoverers, Joiners, and Sentinels;

Discoverers and Joiners can switch between each other, but the proportion of discoverers and joiners in the sparrow population remains constant. Additionally, discoverers possess higher energy reserves (energy storage level depends on the individual's fitness value);

When Sentinels in the sparrow population detect predators, they start chirping and move towards a safe area. If the sentinel's warning exceeds a certain threshold, the discoverers will lead the joiners to the safe area for foraging;

When the energy of joiners becomes too low, their foraging positions are likely to be lower, increasing the probability of

them flying to other locations for foraging to obtain better energy.

Based on the above rules, construct a mathematical model of the SSA:

$$X = \begin{bmatrix} x_{1,1} & x_{1,2} & \cdots & x_{1,d} \\ x_{2,1} & x_{2,2} & \cdots & x_{1,d} \\ \vdots & \vdots & \vdots & \vdots \\ x_{n,1} & x_{n,2} & \cdots & x_{n,d} \end{bmatrix}$$

When n represents the number of sparrows, d denotes the dimensionality of the variables in the optimization problem, X is sparrow population distribution. $x_{n,d}$ show the coordinates of the n sparrow in the d dimension.

The expression for Tent chaotic map is as follows:

$$x_{i,j}^{k+1} = \begin{cases} x^{k+1} = 2 \cdot r \cdot x^k & 0 \le x^k < \frac{1}{2} \\ x^{k+1} = 2 \cdot r \cdot (1 - x^k) & \frac{1}{2} \le x^k < 1 \end{cases} \tag{10}$$

where r is a control parameter that determines the nature of the chaotic map. k is the number of iterations.

The new population matrix obtained through the tent mapping algorithm is:

$$X^{k+1} = \begin{bmatrix} x_{1,1}^{k+1} & x_{1,2}^{k+1} & \cdots & x_{1,d}^{k+1} \\ x_{2,1}^{k+1} & x_{2,2}^{k+1} & \cdots & x_{1,d}^{k+1} \\ \vdots & \vdots & \vdots & \vdots \\ x_{n,1}^{k+1} & x_{n,2}^{k+1} & \cdots & x_{n,d}^{k+1} \end{bmatrix}$$

Fitness Function of Tent-SSA: In this article, the absolute error between the predicted output (y_i) and the expected output (o_i) is used as the fitness value of an individual. The calculation formula is as follows:

$$F_x = \sum_{i=1}^{n} (abs(y_i - o_i)) \tag{11}$$

In Tent-SSA, the update rule for the position of discoverers is described as follows:

$$x_{i,j}^{k+1} = \begin{cases} x_{i,j}^k \cdot \exp(-\dfrac{i}{\alpha \cdot k_{\max}}) & if\ R_2 \le ST \\ x_{i,j}^k + Q \cdot L & if\ R_2 > ST \end{cases} \tag{12}$$

where $x_{i,j}^k$ denotes the position of the i-th sparrow in the j-th dimension during the k-th iteration. α is a random number ((0, 1]). L indicates a $1 \cdot d$ matrix, and its element are all 1. Meanwhile, when $R_2 \le ST$, it indicates that the sparrows are in a safe state. When $R_2 > ST$, it signifies that the sparrows have detected the predators and begin emitting warning signals.

The operating formula for the joiners is as follows:

$$x_{i,j}^{k+1} = \begin{cases} Q \cdot \exp(\dfrac{X_w - X_{i,j}^k}{i^2}) & if\ i > \frac{n}{2} \\ X_b^{k+1} + \left| X_{i,j}^k - X_b^{k+1} \right| \cdot A^+ \cdot L & otherwise \end{cases} \tag{13}$$

where X_b, X_w are the current best position and the worst position of the discoverer sparrow individual. A is a matrix containing elements of 1 or -1, and $A^+ = A^T(AA^T)^{-1}$. When $i > \frac{n}{2}$, it indicates that the i-th joiner sparrow has not found food and needs to move to another area.

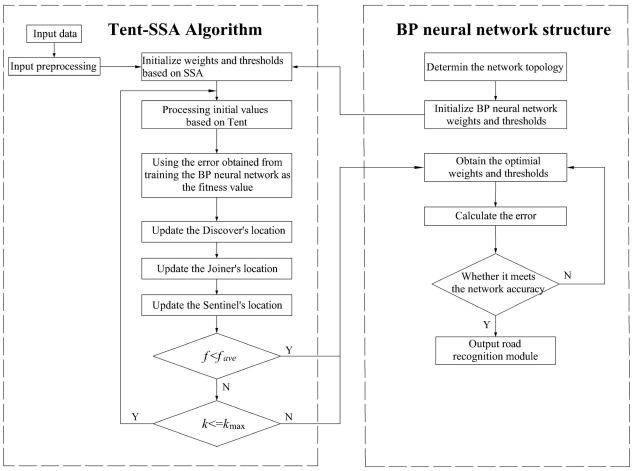

FIGURE 10. The structure of RR module.

The formula for the sentinel is as follows:

$$X_{i,j}^{k+1} = \begin{cases} X_b^k + \rho \cdot \left| X_{i,j}^k - X_b^k \right| & if\ f_i > f_b \\ X_{i,j}^k + R \cdot (\dfrac{\left| X_{i,j}^k - X_w^k \right|}{(f_i - f_w) + \varepsilon}) & if\ f_i = f_b \end{cases} \tag{14}$$

In the equations: ρ is the step control parameter following a normal distribution; f_i represents the current individual fitness value; f_b, f_w are the current best and worst fitness values, respectively. ε is the minimum constant to avoid a denominator of zero. $R \in [-1, 1]$ is a random number. When $f_i > f_b$, it indicates that the sparrow individual is located at the boundary of the population's position, making it susceptible to predation. When $f_i = f_b$, it signifies that the sparrow individual is aware of the danger and needs to move closer to other individuals in the population.

Fig.10 illustrates the design process of Tent-SSA-BP within the entire RR module.

To simulate the $\ddot{z}_2, \ddot{\theta}, \Delta x$ under various road conditions, vehicle suspension model is created in MATLAB. These simulations produce training sample data. A learning rate of 0.005 to train the input and output data with the Levenberg-Marquardt algorithm. The trained neural network model is utilized to calculate the probabilities of each road condition corresponding to the input data. The road condition with the highest probability is considered the final output, thus completing the road condition recognition.

This article applies the road recognition module to four freedom suspension models. Fig.11 displays the comparative results between simulated fluctuation in suspension vibration signals transformed by the Tent-SSA-BP neural network and actual road on B-grade and E-grade road surfaces.

Based on the above road simulation, we can observe that the simulation accuracy is relatively high on smooth road surfaces (B-grade road), but efficiency significantly decreases

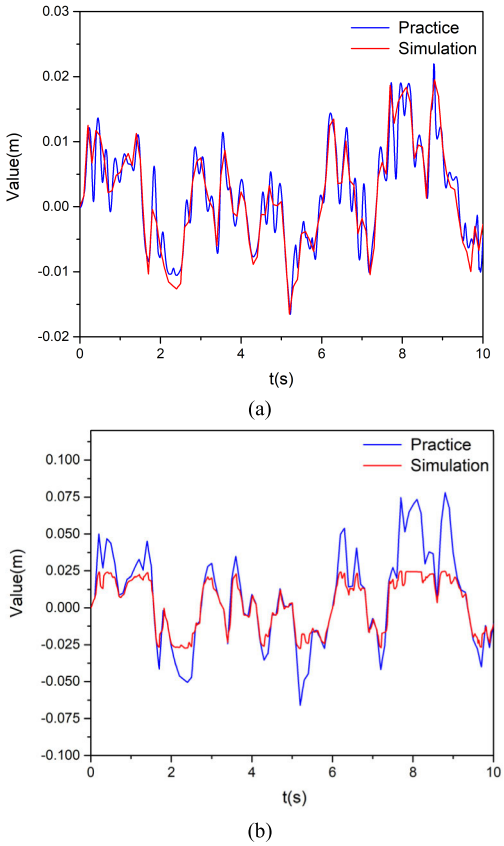

FIGURE 11. The comparative results between simulated fluctuation in suspension vibration signals and actual road; (a) The simulation results for B-grade road; (b) The simulation results for E-grade road.

when operating on complex road surfaces (E-grade road). The extent of decrease varies across different complex road surfaces, and the recognition accuracy is also influenced by the driving speed. Overall, the assessment has decreased by 20% to 30%. Additionally, the recognition efficiency of the BP neural network on complex road surfaces has declined by 14.21% compared to the Tent-SSA-BP neural network in Fig.12.

C. PID TUNING COEFFICIENT OPTIMIZING BASED ON CPSO

The PSO algorithm is widely used in solving multi-constraint optimization and non-linear optimization problems, which is a typical evolutionary computation method based on the collective behavior of particles. It has advantages such as simplicity in concept and ease of implementation. However, it also has some apparent drawbacks, including slow convergence speed and a tendency to get stuck in local optima.

To address the issue of local optima in the PSO algorithm, this study introduces chaotic theory. It uses chaotic mapping to embed particle position information during the initialization of the particle swarm. This approach reduces the problem of particles being concentrated locally during the random generation of particles at the beginning, thus improving the

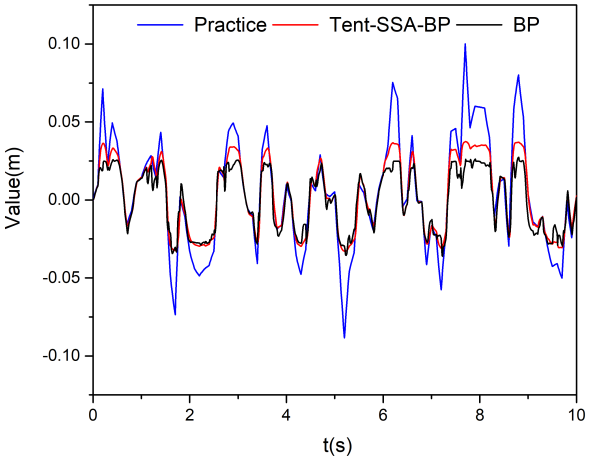

FIGURE 12. The comparative results between Tent-SSA-BP and BP in E-grade road.

diversity of particle search and avoiding being trapped in local optima.

The mathematical description of the PSO algorithm is as follows:

Consider a population $x = (x_1, x_2, \ldots x_n)^T$ is composed of n particles in a D-dimensional search space, where the position of i-th particle is $x_i = (x_{i1}, x_{i2}, \cdots, x_{id})^T$ with a speed of $v_i = (v_{i1}, v_{i2}, \cdots, v_{id})^T$. Its individual extreme value $p_i = (p_{i1}, p_{i2}, \cdots, p_{id})^T$, and the global extreme value of the population is $p_g = (p_{g1}, p_{g2}, \cdots, p_{gn})^T$. The speed and position of each particle are then determined based on (13) and (14), respectively, after getting those two extreme values.

$$v_{id}^{k+1} = \omega \cdot v_{id}^{k} + c_1 \cdot rand() \cdot (p_{id}^{k} - x_{id}^{k}) + c_2 \cdot rand() \cdot (p_{gd}^{k} - x_{id}^{k}) \quad (15)$$

$$x_{id}^{k+1} = x_{id}^{k} + v_{id}^{k+1} \quad (16)$$

The above section explained the basic concept and operational logic of PSO. Now, the specific implementation process of the improved and optimized PSO algorithm based on chaotic theory will be presented as follows:

1) SETTING OF THE LEARNING-FACTOR

In the early stages of population search, the emphasis is on individual experience, favouring exploration of the search space. As the population evolves, collective experience plays a greater role, indicating that the learning factor's parameters should decrease over time. Therefore, in this study, the Learning-Factor is defined using a linear function that continuously reduces according to the number of iterations until reaching its minimum value. The Learning-Factor is confined within the interval [1.75, 2.15]. The initial values of s_1, s_2 are set to 1.75, c_1, c_2 are set to 2.15. Hence, the learning factors ω_1, ω_2 are as follows:

$$\omega_1 = c_1 - (c_1 - s_1) \cdot (k/k_{\max}) \quad (17)$$

$$\omega_2 = c_2 - (c_2 - s_2) \cdot (k/k_{\max}) \quad (18)$$

2) SETTING OF THE INERTIA FACTOR

The inertia weight ω is a crucial parameter in the PSO algorithm. Increasing the value of ω enhances the algorithm's global search capability, while decreasing it improves the local search capability. Therefore, in the PSO algorithm, the inertia weight factor is continuously reduced. In this study, a nonlinear dynamic inertia weight coefficient formula is constructed using the inverse cosine function to update the inertia factor. This ensures that the inertia weight is dynamically adjusted within the range [0.4, 0.8] in a nonlinear manner. The formula is as follows:

$$\omega = \omega_{\min} + (\omega_{\max} - \omega_{\min}) \cdot \frac{2}{\pi} \cdot \arccos(\frac{k}{k_{\max}}) \tag{19}$$

3) FITNESS EVALUATION METHOD

Considering the inconsistent units and magnitudes of the performance indicators VBVA ($\ddot{z}_2$) PAA ($\ddot{\theta}$) and FSD (Δx). This study divides them by the corresponding passive suspension performance indicators to obtain the corresponding fitness values. The optimization problem is expressed as follows:

$$\min J = \frac{VBVA(H)}{VBVA_{ps}} + \frac{PAA(H)}{PAA_{ps}} + \frac{FSD(H)}{FSD_{ps}} \tag{20}$$

$$s.t. = \begin{cases} VBVA < VBVA_{ps} \\ PAA < PAA_{ps} \\ FSD < FSD_{ps} \end{cases} \tag{21}$$

When $H = \begin{bmatrix} q_p & q_i & q_d \end{bmatrix}$ represents the correction coefficients. The fitness is continuously obtained through (20), while simultaneously checking if the constraint condition (21) is satisfied. If all constraints are met, the fitness value J is output. Otherwise, the fitness function value J is increased by 10 to move it away from the evolutionary direction constrained by the population.

4) SETTING OF THE CHAOTIC ALGORITHM

The quality of the population during the initialization phase directly affects the performance of the algorithm; PSO algorithm typically adopts random initialization to generate the initial population, but this method has high randomness and poor diversity, leading to the inability of the population to achieve uniform distribution in the search space. Therefore, introducing Logistic map becomes necessary. The formula is as follows:

$$z_{k+1} = \mu \cdot z_k(1 - z_k) \tag{22}$$

In addition, incorporating the chaotic operator allows the PSO algorithm to fluctuate within a certain range when trapped in a local optimal solution, thereby reducing the sensitivity to the optimal solution and improving its performance.

$$\delta x_{k+1} = \sin(\pi \cdot \delta x_k) \tag{23}$$

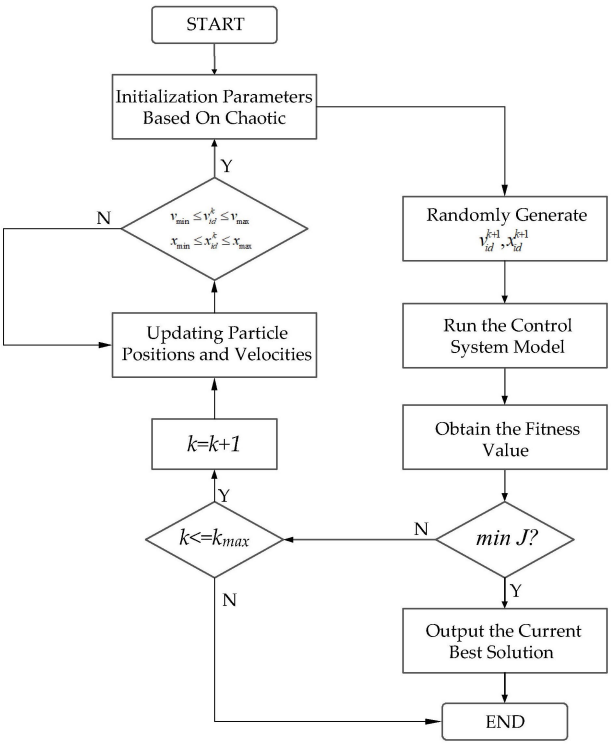

FIGURE 13. The structure of CPSO.

5) THE UPDATE EQUATIONS

Combining the above formulas, the position and velocity update equations for the particle swarm are as follows:

$$v_{id}^{k+1} = \omega \cdot v_{id}^{k} + \omega_1 \cdot rand() \cdot \left[p_{i,j}^{k} - x_{i,j}^{k}\right] + \omega_2 \cdot rand() \cdot \left[p_{g,j}^{k} - x_{i,j}^{k}\right] \tag{24}$$

$$x_{id}^{k+1} = x_{id}^{k} + v_{id}^{k+1} + \Delta\delta x_{k+1} \tag{25}$$

The steps and workflow of the improved algorithm are summarized as follows, as shown in Fig.13.

1) Initialize Parameters: Generate the initial population based on (22). Set the learning factor and inertia weight factor using (17,18) and (19), respectively. Determine the total number of particles, maximum iteration count $k_{\max}$, and define the parameter ranges.

2) Generate Particle Positions and Velocities using (15) and (16).

3) Evaluate Fitness and Constraint Particles: Calculate the fitness and constraint values of particles using (20) and (21). Store the best position and corresponding fitness value of each particle, as well as the best position and fitness value of the entire population.

4) Conduct Simulation: Implement the optimization by importing the best individual and global best positions into the simulation and iteratively optimizing.

5) Update Particle Position and Velocity: Update the position and velocity of each particle using (24) and (25).

6) Update Personal and Global Best: Compare the fitness values with the current best positions of each particle. If they

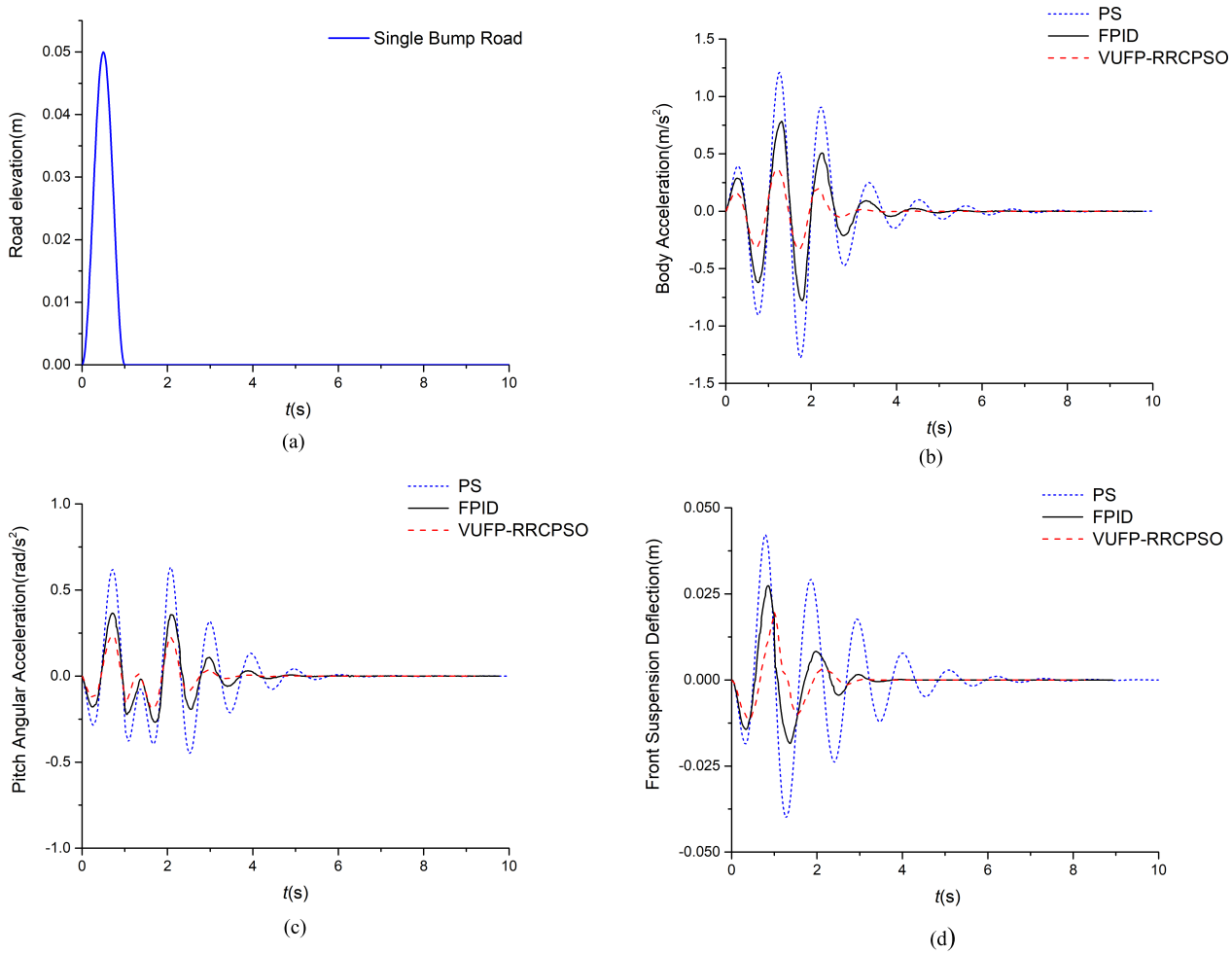

FIGURE 14. Comparison of Suspension Control Performance on Single Bump Road. (a) The Single Bump Road; (b) VBVA under Bump Road. (c) PAA under Bump Road. (d) FSD under Bump Road.

are close, update the current value as the particle's personal best position.

7) Check Termination Condition: Check if the $k_{\max}$ count has been reached. If yes, end the optimization; otherwise, return to step 2.

IV. SIMULATION AND ANALYSIS

For proof of the efficiency of the control Strategy in the article, MATLAB/Simulink is applied to simulate the ASS and test the vibration reduction performance of various control strategies under multiple road circumstances (Single Bump Road, Sinusoid Road, Random Road). The three indicators $\ddot{z}_2, \ddot{\theta}, \Delta x$ mentioned above, are utilized as assessment indicators. Table 5 details the suspension system's parameters.

Create a road with a single bump as follows:

$$q(t) = \begin{cases} \frac{H}{2}\left[1 - \cos(2\pi \frac{v}{L})\right], & 0 \le t \le \frac{L}{v} \\ 0 & t > \frac{L}{v} \end{cases} \tag{26}$$

where H, L, v respectively represent the height, length, and forward speed of the bump, and their values are set as A = 0.05 m, L = 10 m, and v = 10 m/s.

TABLE 5. The parameter of vehicle suspension.

Symbol	Value	Unit	Symbol	Value	Unit
m_s	1235	Kg	k_f	22741	N·m-1
m_f	49	Kg	k_r	22741	N·m-1
m_r	49	Kg	k_{tf}	302342	N·m-1
a	1.2	m	k_{tr}	492982	N·m-1
b	1.5	m	c_f	1221	N·s·m-1

A simulated road surface is built based on the formula above for a single convex road surface, and it is used as a simulation model for road conditions. The simulation results are shown in the following figure.

The control strategy is applied to the Active suspension and the automobile is driven on a single hump road to more accurately assess the suspension control performance of the PS, FPID, and VUFP-RRCPSO. These figures demonstrate

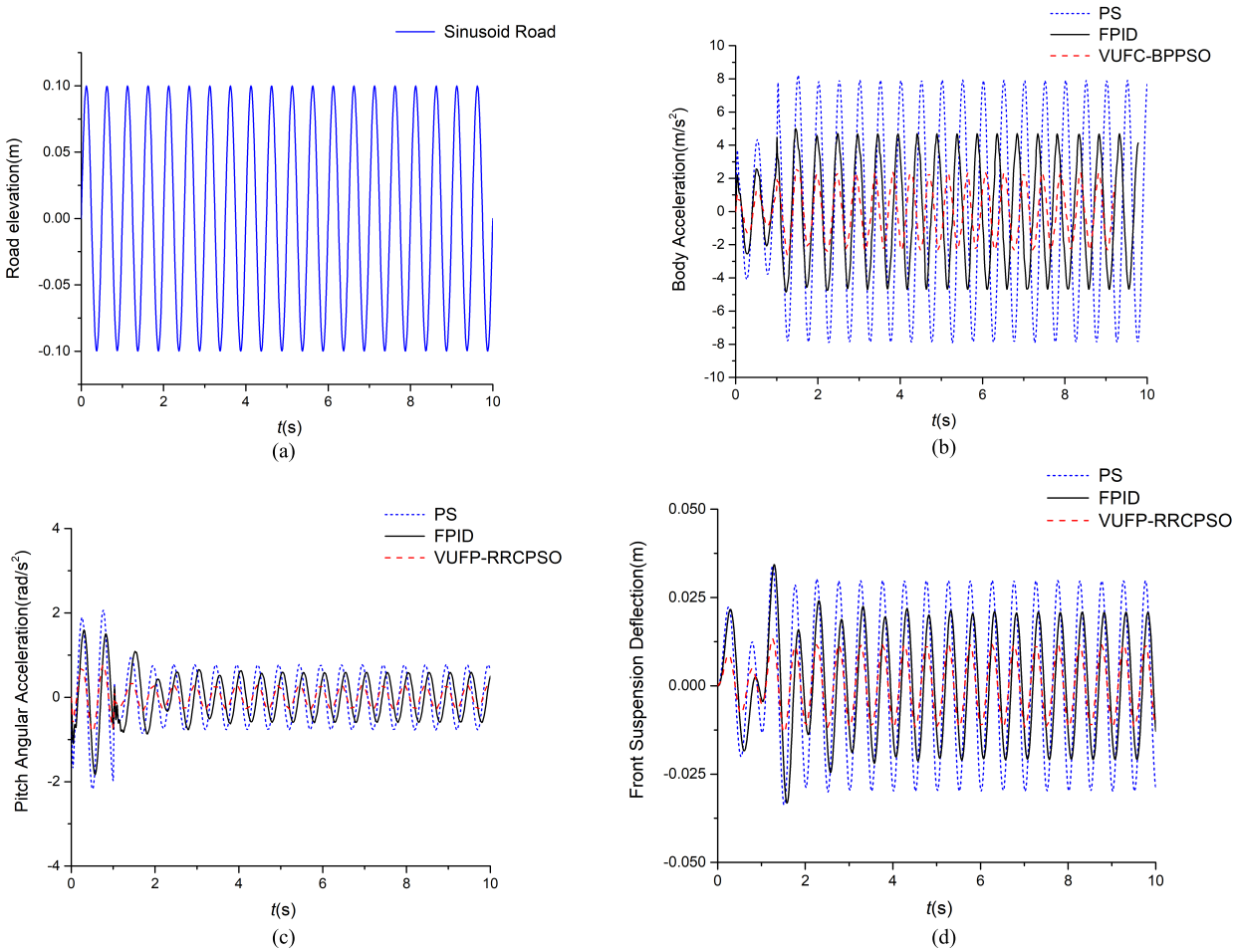

FIGURE 15. Comparison of Suspension Control Performance on Sinusoid Road. (a) The Sinusoid Road; (b) VBVA under the Sinusoid Road. (c) PAA under the Sinusoid Road. (d) FSD under the Sinusoid Road.

TABLE 6. RMS value of suspension evaluation metric on bump road.

Signal	Control Strategy		
	PSS	FPID	VUFP-RRCPSO
$\ddot{z}_2$	0.4077	0.2558	0.1818
$\ddot{\theta}$	0.2056	0.1386	0.0963
Δx	0.0136	0.0091	0.0067

TABLE 7. RMS value of suspension evaluation metric on sinusoid road.

Signal	Control Strategy		
	PSS	FPID	VUFP-RRCPSO
$\ddot{z}_2$	3.1099	2.6118	1.7639
$\ddot{\theta}$	0.6679	0.5786	0.4185
Δx	0.1994	0.1481	0.1184

that VUFP-RRCPSO can markedly decreased VBVA, PAA and FSD. The particular data is displayed in Table 6.

As indicated in Table 6, compared to the PSS and FPID controllers, the VUFP-RRCPSO controllers has reduced the VBVA, PAA, and FSD indices by 55.41%, 53.16%, 50.74%, and 28.92%, 30.52%,26.37%, respectively. This indicates that the VUFP-RCPSO controller has superior responsiveness and vibration reduction capabilities when facing sudden vibrations.

Create a Sinusoid Road as follows:

The chosen road is a sinusoidal one with a 2 Hz frequency and a 0.05 m amplitude. One way to describe a sinusoidal road is as follows:

$$q(t) = 0.05 \cdot \sin 4\pi t \tag{27}$$

When using VUFP-RRCPSO controllers driven on a sinusoid road, the RMS values of VBVA, PAA, and FSD fell by approximately 32.46%, 27.67%, 20.06%, and 43.28%, 37.34%, 40.62%, compared to the PSS and FPID controllers, as illustrated in Table 7.

Based on these results, the VUFP-RRCPSO controllers demonstrates superior performance in maintaining control on a sinusoidal road.

Create a random road surface based on formula (9):

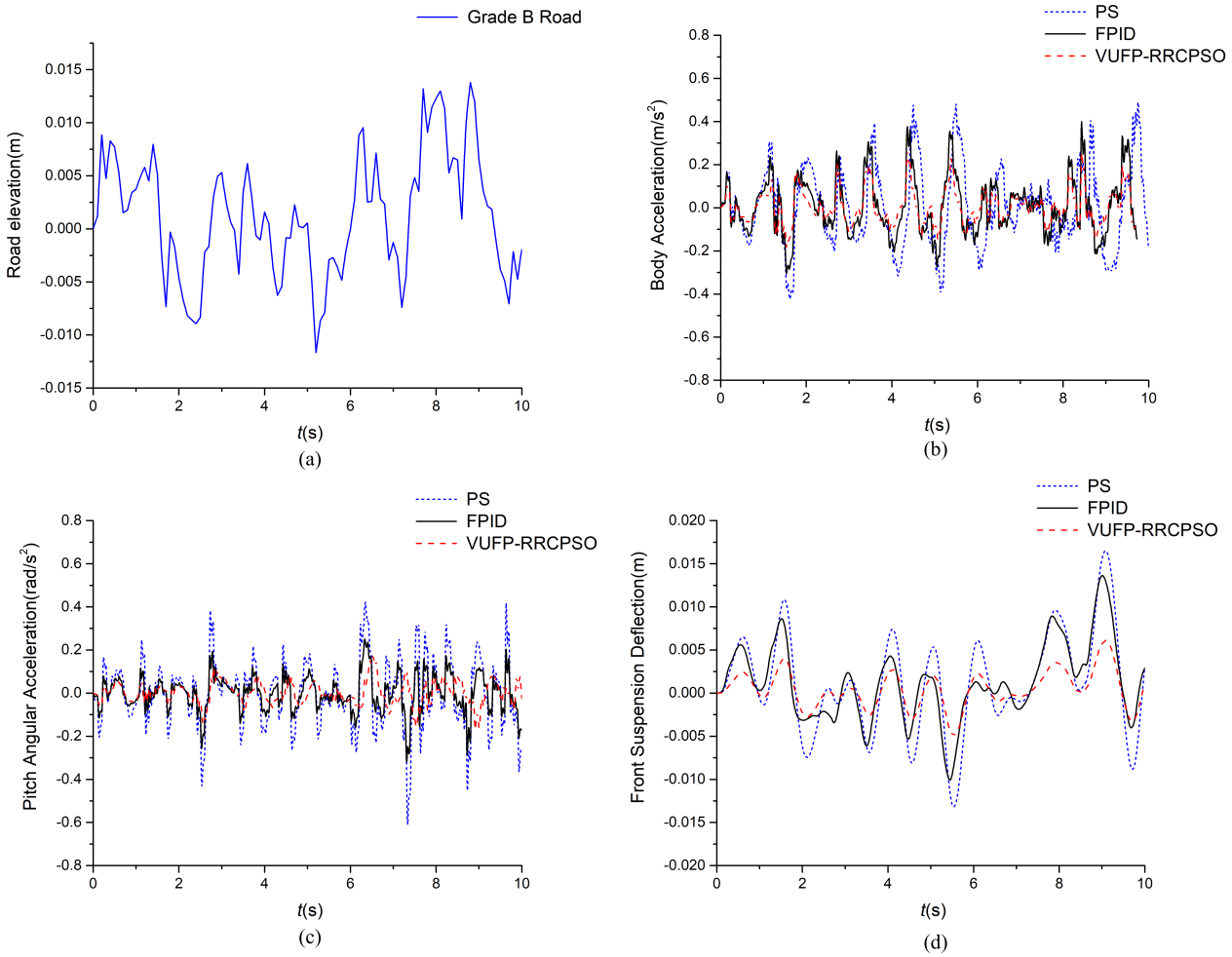

FIGURE 16. Comparison of Suspension Control Performance on B Random Road. (a) The B Random Road; (b) VBVA under B Random Road. (c) PAA under the B Random Road. (d) FSD under the B Random Road.

TABLE 8. RMS value of suspension evaluation metric on sinusoid road.

Signal	Control Strategy		
	PSS	FPID	VUFP-RRCPSO
$\ddot{z}_2$	0.1852	0.1418	0.0922
$\ddot{\theta}$	0.1561	0.1173	0.0829
Δx	0.0058	0.0046	0.0032

The control strategy is applied to the ASS and driven on B Random Road. In the meantime. These figures demonstrate that VUFP-RRCPSO can significantly reduce VBVA, PAA and FSD. Compared with PS and FPID, when using the VUFP-RRCPSO controller, the RMS values of VBVA, PAA, and FSD decreased by approximately 34.97%, 24.86%, 30.43%, and 50.21%, 46.89%, 44.83%, respectively. According to this outcome, the proposed controller works better when it comes to maintaining control on Random Road.

From the above three road simulation results, it can be observed that the comprehensive performance of the VUFP-RRCPSO controllers have improved by 28.47% compared to the FPID control strategy on different road surfaces.

V. CONCLUSION

Fuzzy PID controller, the most widely used controller in suspension systems, has high practical value in enhancing vehicle safety. However, the fuzzy PID controllers suffer from fixed universes and road excitation. To overcome these limitations and enhance control performance, the universe fuzzy PID control strategy combining road recognition and chaotic particle swarm optimization is proposed in this research. In this strategy, to generate a dataset of corresponding to different road conditions, the road grade is combined with the suspension vibration information. The dataset is used to train a Tent-SSA-BP neural network and construct a road recognition module. Meanwhile, the contraction-expansion factors are obtained for different vehicle accelerations by variable universe rules. The road recognition adapts and adjusts the contraction-expansion factors based on the sensed suspension information, which avoiding the fixed universe. Additionally, the control system incorporates the CPSO to optimize the tuning parameter of the FPID controller, improving output

accuracy and reducing the influence of expert experience. The results demonstrate the proposed control strategy has improved the three metrics of vertical acceleration, pitch angular acceleration, and front suspension displacement by 30.087%, 26.73%, and 28.603%, respectively, compared to the fuzzy PID control.

In future research can further deepen understanding of artificial intelligence and better apply neural networks and intelligent algorithms to automotive suspension technology.

REFERENCES

[1] H. E. Tseng and D. Hrovat, "State of the art survey: Active and semi-active suspension control," *Vehicle Syst. Dyn.*, vol. 53, no. 7, pp. 1034–1062, Jul. 2015, doi: 10.1080/00423114.2015.1037313.

[2] J. Lin and R.-J. Lian, "Intelligent control of active suspension systems," *IEEE Trans. Ind. Electron.*, vol. 58, no. 2, pp. 618–628, Feb. 2011, doi: 10.1109/TIE.2010.2046581.

[3] Y. Huang, J. Na, X. Wu, X. Liu, and Y. Guo, "Adaptive control of nonlinear uncertain active suspension systems with prescribed performance," *ISA Trans.*, vol. 54, pp. 145–155, Jan. 2015, doi: 10.1016/j.isatra.2014.05.025.

[4] L. Khan, S. Qamar, and U. Khan, "Adaptive PID control scheme for full car suspension control," *J. Chin. Inst. Eng.*, vol. 39, no. 2, pp. 169–185, Feb. 2016, doi: 10.1080/02533839.2015.1091427.

[5] A. B. Sharkawy, "Fuzzy and adaptive fuzzy control for the automobiles' active suspension system," *Vehicle Syst. Dyn.*, vol. 43, no. 11, pp. 795–806, Nov. 2005, doi: 10.1080/00423110500097783.

[6] P. Guarneri, G. Rocca, and M. Gobbi, "A neural-network-based model for the dynamic simulation of the tire/suspension system while traversing road irregularities," *IEEE Trans. Neural Netw.*, vol. 19, no. 9, pp. 1549–1563, Sep. 2008, doi: 10.1109/TNN.2008.2000806.

[7] H. Zhou, Y. Li, H. Xu, Y. Su, and L. Chen, "A self-organizing fuzzy neural network modeling approach using an adaptive quantum particle swarm optimization," *Int. J. Speech Technol.*, vol. 53, no. 11, pp. 13569–13592, Jun. 2023, doi: 10.1007/s10489-022-04133-8.

[8] H. Pang, F. Liu, and Z. Xu, "Variable universe fuzzy control for vehicle semi-active suspension system with MR damper combining fuzzy neural network and particle swarm optimization," *Neurocomputing*, vol. 306, pp. 130–140, Sep. 2018, doi: 10.1016/j.neucom.2018.04.055.

[9] J. Na, Y. Huang, X. Wu, S.-F. Su, and G. Li, "Adaptive finite-time fuzzy control of nonlinear active suspension systems with input delay," *IEEE Trans. Cybern.*, vol. 50, no. 6, pp. 2639–2650, Jun. 2020, doi: 10.1109/TCYB.2019.2894724.

[10] M. Liu, Y. Zhang, J. Huang, and C. Zhang, "Optimization control for dynamic vibration absorbers and active suspensions of in-wheel-motor-driven electric vehicles," *Proc. Inst. Mech. Eng., D, J. Automobile Eng.*, vol. 234, no. 9, pp. 2377–2392, Aug. 2020, doi: 10.1177/0954407020908667.

[11] P. Swethamarai and P. Lakshmi, "Adaptive-fuzzy fractional order PID controller-based active suspension for vibration control," *IETE J. Res.*, vol. 68, no. 5, pp. 3487–3502, Sep. 2022, doi: 10.1080/03772063.2020.1768906.

[12] P. Nitsche, R. Stütz, M. Kammer, and P. Maurer, "Comparison of machine learning methods for evaluating pavement roughness based on vehicle response," *J. Comput. Civil Eng.*, vol. 28, no. 4, Jul. 2014, Art. no. 04014015, doi: 10.1061/(asce)cp.1943-5487.0000285.

[13] A. E. Baumal, J. J. McPhee, and P. H. Calamai, "Application of genetic algorithms to the design optimization of an active vehicle suspension system," *Comput. Methods Appl. Mech. Eng.*, vol. 163, nos. 1–4, pp. 87–94, Sep. 1998, doi: 10.1016/s0045-7825(98)00004-8.

[14] M. H. A. Talib, I. Z. M. Darus, P. M. Samin, H. M. Yatim, M. I. Ardani, N. M. R. Shaharuddin, and M. S. Hadi, "Vibration control of semi-active suspension system using PID controller with advanced firefly algorithm and particle swarm optimization," *J. Ambient Intell. Humanized Comput.*, vol. 12, no. 1, pp. 1119–1137, Jan. 2021, doi: 10.1007/s12652-020-02158-w.

[15] A. Hamza and N. Ben Yahia, "Heavy trucks with intelligent control of active suspension based on artificial neural networks," *Proc. Inst. Mech. Eng., I, J. Syst. Control Eng.*, vol. 235, no. 6, pp. 952–969, Jul. 2021, doi: 10.1177/0959651820958516.

[16] I. Dridi, A. Hamza, and N. Ben Yahia, "Control of an active suspension system based on long short-term memory (LSTM) learning," *Adv. Mech. Eng.*, vol. 15, no. 2, Feb. 2023, Art. no. 168781322311567, doi: 10.1177/16878132231156789.

[17] B. Spencer, S. Dyke, M. Sain, and J. Carlson, "Phenomenological model for magnetorheological dampers," *J. Eng. Mech. Arch.*, vol. 123, no. 3, pp. 230–238, Mar. 1997, doi: 10.1061/(ASCE)0733-9399(1997)123:3(230).

[18] M. Zhu, G. Lv, C. Zhang, J. Jiang, and H. Wang, "Delay-dependent sliding mode variable structure control of vehicle magneto-rheological semi-active suspension," *IEEE Access*, vol. 10, pp. 51128–51141, 2022, doi: 10.1109/ACCESS.2022.3173605.

[19] H.-X. Li, Z.-H. Miao, and E. S. Lee, "Variable universe stable adaptive fuzzy control of a nonlinear system," *Comput. Math. Appl.*, vol. 44, nos. 5–6, pp. 799–815, Sep. 2002.

[20] F. Herrera, M. Lozano, and J. L. Verdegay, "A learning process for fuzzy control rules using genetic algorithms," *Fuzzy Sets Syst.*, vol. 100, nos. 1–3, pp. 143–158, Nov. 1998.

[21] F. Tyan, Y.-F. Hong, S.-H. Tu, and W. S. Jeng, "Generation of random road profiles," *J. Adv. Eng.*, vol. 4, no. 2, pp. 1373–1378, 2009.

[22] A. González, E. J. O'brien, Y.-Y. Li, and K. Cashell, "The use of vehicle acceleration measurements to estimate road roughness," *Vehicle Syst. Dyn.*, vol. 46, no. 6, pp. 483–499, Jun. 2008, doi: 10.1080/00423110701485050.

[23] H. Zhou, Y. Li, Q. Zhang, H. Xu, and Y. Su, "Soft-sensing of effluent total phosphorus using adaptive recurrent fuzzy neural network with Gustafson–Kessel clustering," *Expert Syst. Appl.*, vol. 203, Oct. 2022, Art. no. 117589, doi: 10.1016/j.eswa.2022.117589.

[24] J. Mikulić and D. Prebežac, "Accounting for dynamics in attribute-importance and for competitor performance to enhance reliability of BPNN-based importance-performance analysis," *Expert Syst. Appl.*, vol. 39, no. 5, pp. 5144–5153, Apr. 2012, doi: 10.1016/j.eswa.2011.11.026.

[25] J. Xue and B. Shen, "A novel swarm intelligence optimization approach: Sparrow search algorithm," *Syst. Sci. Control Eng.*, vol. 8, no. 1, pp. 22–34, Jan. 2020, doi: 10.1080/21642583.2019.1708830.

WANGSHUI YU received the B.S. degree from Jiangsu Ocean University, China. He is currently pursuing the master's degree with Jiangsu University of Technology. His current research interests include vehicle dynamics and automation control.

KAI ZHU received the Ph.D. degree in control science and control engineering from Nanjing University of Science and Technology, in 2015. He is currently a Teacher with the School of Automobile and Traffic Engineering, Jiangsu University of Technology. His research interests include application of big data and intelligent transportation systems.

YATING YU received the B.S. degree from Jiangsu University of Technology, China, where she is currently pursuing the master's degree. Her current research interests include visual slam, deep learning, and digital image processing.